Short-Term versus Climatological Relationship between Precipitation and Tropospheric Humidity

Hirohiko Masunaga

Hydrospheric Atmospheric Research Center, Nagoya University, Nagoya, Japan

ABSTRACT

In this study the observed relationship of precipitation with column relative humidity (CRH), a metric of tropospheric humidity, is examined in order to address a known discrepancy inherent to past studies. A composite analysis of satellite data is carried out to explore the short-term (i.e., from hourly to daily) atmospheric variability for comparison with the climatology, hypothesizing that a primary cause for the discrepancy arises from a difference in the time scale of interest. The analysis is broken down into four classes on the basis of the degree of convective organization, ranging from unorganized shallow cumuli to highly organized convective systems. The CRH–precipitation relationship is found to be extremely nonlinear for the short-term variability, while the nonlinearity weakens to some degree when different convective systems in diverse humidity environments are averaged together into climatology. The weak exponential rise in the climatological CRH–precipitation curve occurs because highly organized convective systems become more frequent and intense and thus receive increasing weight in the climatological mean as the environment moistens.

1. Introduction

While the initiation of vigorous convection critically relies on moist air in the atmospheric boundary layer, the free-tropospheric moisture is also known to be another key parameter of tropical moist convection (e.g., Numaguti et al. 1995; Brown and Zhang 1997; Sherwood 1999; Raymond 2000; Derbyshire et al. 2004; Holloway and Neelin 2009). Satellite microwave radiometry provides a good estimate of the tropospheric water vapor or column water vapor (CWV) and precipitation over ocean and has been widely used for studying the observed link between the tropospheric moisture and precipitation. From satellite data analysis, Bretherton et al. (2004) showed that precipitation statistically falls into a regionally insensitive exponential function of column relative humidity (CRH; also known as saturation fraction) or the ratio of CWV to the vertically integrated saturation vapor density. A similar nonlinear relationship between precipitation and CRH was confirmed in in situ sounding data analyzed by Raymond et al. (2007), although the nonlinearity there turned out to be much

stronger than found by Bretherton et al. (2004) (Raymond et al. 2011). The present work discusses the origins of this apparent discrepancy.

Satellite and ground measurements are different in temporal and spatial resolution, which is likely one of the factors that gives rise to the discrepancy. In situ soundings are optimal for detecting the short-term variability at the expense of a limitation to the areal coverage or universality of the data. Satellite data are of great utility for homogeneous sampling over the globe beyond the reach of ground-based observations. A major challenge to satellite remote sensing, however, is that satellites in low Earth orbit (LEO) are limited in capability to sample anything varying faster than the satellite revisit frequency (typically twice daily). In attempt to avoid this difficulty, Masunaga (2012) devised an analysis method to combine observations by two LEO satellites so that a statistically continuous composite time series of atmospheric variability is obtained. The present study exploits this analysis strategy to achieve a high temporal resolution (in a statistical sense) comparable to typical ground measurements.

Peters and Neelin (2006) and their subsequent work (Neelin et al. 2009; Peters et al. 2009) showed that the transition to strong tropical convection and resultant drying processes are clearly captured in satellite observations as a sharp increase in rainfall and a decrease in its population

Corresponding author address: Hirohiko Masunaga, Hydrospheric Atmospheric Research Center, Nagoya University, Furocho, Chikusa-ku, Nagoya 464-8601, Japan.
E-mail: masunaga@hyarc.nagoya-u.ac.jp

above a critical point of CWV. Potential implications of this study for these findings will be also briefly discussed.

Data and analysis methodology are described in section 2. Results are presented in section 3 and discussed in section 4.

2. Data and methods

The present analysis exploits a combination of two satellites in different (i.e., sun-synchronous and asynchronous) orbits to obtain composite time series of atmospheric states before and after convection develops. Measurements from one satellite are composited against another, the Tropical Rainfall Measuring Mission (TRMM) satellite in this case, with respect to the observational time difference between the two satellite overpasses. Such time difference changes over time, and a large number of collected samples eventually yields a statistically continuous time series when composited together. The zero on the composite time axis corresponds to the times when the TRMM precipitation radar (PR) detects convection, so that the composite sequence represents the atmospheric variability associated with convective development [see Masunaga (2012) for a detailed description of the methodology].

Convective occurrence defined in this paper is determined by the PR minimum detectability, which is roughly 0.7 mm h^{-1} in rain rate (Kummerow et al. 1998). As noted in Masunaga (2012), a composite time series could be smeared to the degree imposed by the lifetime of convective systems, since the current compositing technique does not pinpoint the peak or any particular stage of the convective life cycle. Although this could challenge the performance of the composite analysis, the sharp cutoff in composite rainfall at $t = 0$ as will be shown in section 3b appears to suggest that the current analysis has the ability to capture changes as brief as a few hours when they occur.

This work adopts the *Aqua* and *CloudSat* satellites, flying as part of the A-Train formation in a 0130 and 1330 local time sun-synchronous orbit, as the counterpart to be composited against the TRMM. The *Aqua* satellite carries the Advanced Microwave Scanning Radiometer for Earth Observing System (AMSR-E) and the Atmospheric Infrared Sounder and Advanced Microwave Sounder Unit (AIRS/AMSU, hereafter called AIRS collectively). The Remote Sensing Systems AMSR-E data products (Wentz and Meissner 2000) provide CWV over global oceans, and the AIRS level-3 daily product (Susskind et al. 2003, 2006) offers air temperature estimates. CRH is obtained from AMSR-E CWV and AIRS air temperature. CRH at $t = 0$ in the composite domain, or hereafter the reference CRH, will be later defined as a measure of humidity environment. The reference CRH,

by definition, must be evaluated from the TRMM instead of the *Aqua* instruments. CWV derived from the TRMM Microwave Imager (TMI), a microwave radiometer similar to the *Aqua* AMSR-E, yields the reference CRH.

Since AIRS temperature is unavailable for fully cloudy scenes, data gaps are filled in by applying a temporal interpolation with a ±1-day running mean to each grid box. This procedure would not introduce a notable error in the CRH estimate since tropical tropospheric temperature is very stable on this time scale (Bretherton et al. 2004). AIRS air temperature is also utilized for evaluating the saturation vapor part of the reference CRH, where a temporal offset between the TRMM and *Aqua* observations can be safely ignored in the temperature estimate for the same reason.

Precipitation is adopted from the AMSR-E Goddard Profiling (GPROF) product (Kummerow et al. 2001). The cloud spatial structure is derived from the *CloudSat* Cloud Profiling Radar (CPR), using the CPR cloud mask (good or strong echoes only) to define cloudiness at different vertical levels. The climatological relationship of precipitation with CRH is derived from the same satellite dataset but without any TRMM-based screening.

All the satellite measurements are averaged to the quarter-degree resolution. The study domain is the whole tropical and subtropical oceans bound between 25°S and 25°N in latitude. The study period is 7+ years from 1 September 2002 to 1 December 2009, except for the *CloudSat* composite where the period spans roughly 3.5 years from 1 July 2006 to the same ending date as above.

Composite diagrams are separated by the degree of convective organization ranging from scattered convection to highly organized systems such as mesoscale convective systems (MCSs). To facilitate this, a surrounding 1° × 1° reference domain with up to 16 PR pixels included is searched for neighboring convective clouds every time when the TRMM PR detects convection. The density of these convective clouds or TRMM precipitation coverage is defined as the number of convective pixels divided by the total number of observed pixels. TRMM precipitation coverage acts as the controlling parameter to break down the analysis into different classes of convective systems (section 3a). Composite time series are binned every half an hour from −48 to +48 h, with the base point ($t = 0$) defined at the time of TRMM detected convection.

3. Results

a. TRMM precipitation coverage and convective organization

The vertical development of clouds from composite *CloudSat* CPR data is shown in this section. The aim
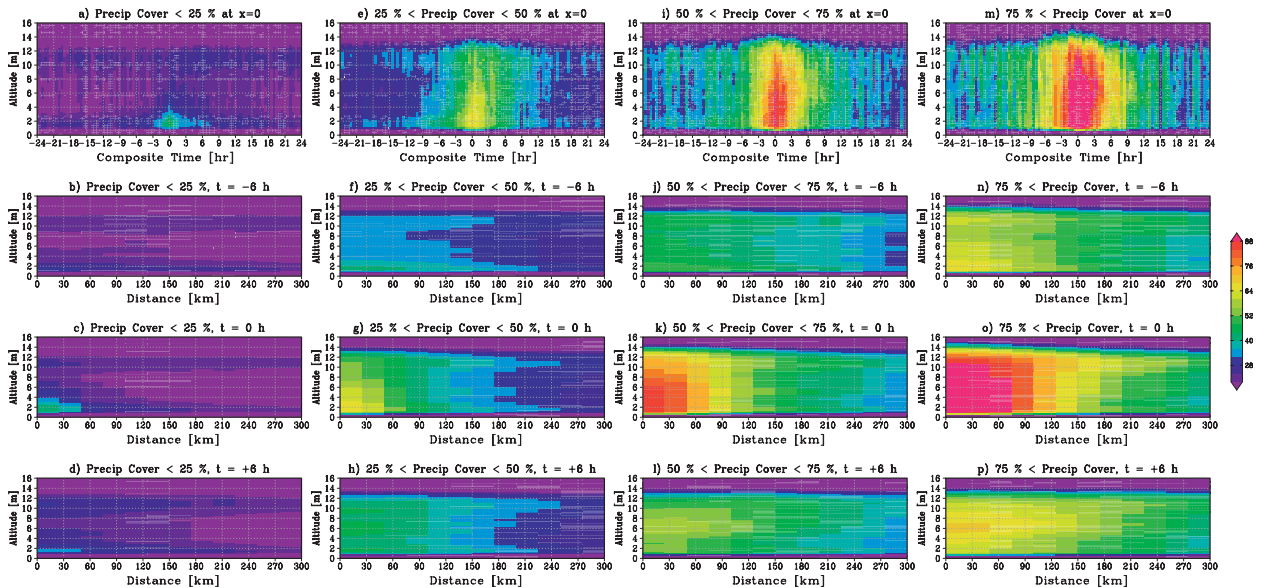
FIG. 1. (a) The composite temporal evolution of *CloudSat* cloudiness and (b)–(d) the spatial structure at selected times ($t = -6$, 0, and 6 h) for TRMM precipitation coverages <25% (exclusive of zero). (e)–(h) As in (a)–(d), but for TRMM precipitation coverages of 25%–50%. (i)–(l) As in (a)–(d), but for TRMM precipitation coverages of 50%–75%. (m)–(p) As in (a)–(d), but for TRMM precipitation coverages of 75%–100%. The spatial structure is the vertical slice of composite *CloudSat* cloudiness at $t = 0$ as a function of distance (km) from the TRMM detected convection.

here is to delineate the temporal evolution of different types of clouds, including both precipitating and non-precipitating ones, associated with the convective development.

TRMM precipitation coverage (see section 2 for definition) is meant here to differentiate a wide spectrum of tropical convection from scattered cumuli to MCSs. To demonstrate this, the temporal and spatial development of cloud structure is diagnosed with *CloudSat* measurements in the composite space. Figure 1a (top left) shows the composite vertical profiles of *CloudSat* cloudiness that are subset for TRMM precipitation coverages of 25% or less (but nonzero), aimed at extracting sporadic convection. *CloudSat* cloudiness in this case stays small as expected, having a modest peak at $t = 0$ emerging momentarily. The cloud top does not reach much beyond the lower or middle troposphere even at the peak, implying that convection in this case mostly consists of shallow cumulus and cumulus congestus unaccompanied by deep convection. It is noted, however, that *CloudSat* signals there could partly arise from precipitation from above where overcast by higher-level clouds and may not entirely represent shallow convection. The spatial structure of the composite cloudiness at $t = -6$, 0, and +6 h is shown in Figs. 1b–d, where a *CloudSat* vertical slice at each moment is plotted as a function of the distance from the TRMM detected convection. Cloudiness never exceeds 50% across the study domain, implying that the

observed area is covered only with unorganized, scattered convection as expected.

The second column in Fig. 1 shows the same composite plots, but for TRMM precipitation coverages between 25% and 50%. In this case, cloud systems undergo a further vertical development from shallow convection to deeper convection at 0 h. Vigorous convection is more evident when composited with respect to even higher TRMM precipitation coverages (third and fourth columns in Fig. 1). The detailed evolution observed in the composite plot is overall as expected from the well-known life cycle of typical MCSs. A developing phase with increasing cloudiness quickly gives way to the mature phase around $t = 0$, when the entire troposphere is occupied by penetrating deep clouds, potentially including both deep convection and precipitating anvil clouds, over a horizontal domain of ~100 km (Figs. 1k,o). An anvil cloud deck continues to extend over a greater horizontal scale while cloudiness begins to diminish in the lower half of the atmosphere (Figs. 1l,p), suggestive of the rain drop reevaporation in stratiform precipitation.

The features shown in Fig. 1 are consistent with existing knowledge as to the temporal and spatial characteristics of different types of tropical convection. It would therefore be safe to assume that TRMM precipitation coverage may be considered as a reasonable measure to identify different classes of convective

Composite sorted by precip cloud cover
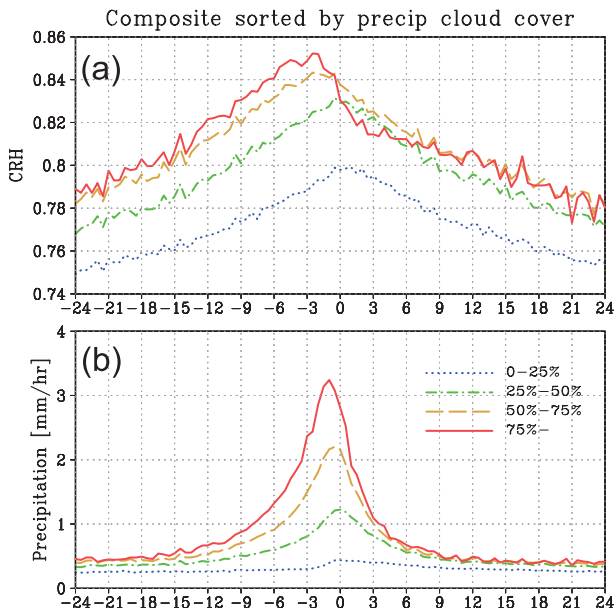

FIG. 2. Composite diagrams of (a) CRH and (b) precipitation, partitioned by different TRMM precipitation coverages of <25% (exclusive of zero), 25%–50%, 50%–75%, and >75%.

systems including scattered convection at one end and highly organized MCSs at the other.

b. CRH and precipitation

The current section is aimed to show the composite time series of CRH and precipitation as derived from *Aqua* AIRS and AMSR-E measurements.

Composite CRH evolution within ± 1 day is shown in Fig. 2a, where CRH is depicted for four precipitation coverage ranges of <25% (exclusive of zero), 25%–50%, 50%–75%, and >75%. All cases agree on that CRH steadily builds up until it peaks near $t = 0$ and then declines as slowly, but they disagree on further details. A notable difference is that highly organized systems (precipitation coverage >75%) experience a quick reduction of CRH during a few hours after the peak, followed by a more gradual drying. In less organized systems, the initial moistening and subsequent drying proceed more smoothly, making the CRH evolution roughly symmetric in time. Composite precipitation picks up quickly within 12 h and then drops down as rapidly (Fig. 2b). A more organized cloud system (or a larger TRMM precipitation coverage) yields a higher precipitation rate at any moment in the composite space.

Holloway and Neelin (2010) studied in situ sounding data and showed that CWV and precipitation each exhibit systematic increase and decrease with a distinct maximum in between, where precipitation is more sharply localized in time than moisture. The present result is overall

consistent with their analysis. Note that the current composite plot would look very similar if CRH is replaced by CWV although CWV is somewhat noisier than CRH (not shown). The overall features presented here are consistent with existing observational studies of the convective life cycle, such as the temporal evolution of precipitable water from Mapes et al. (2009) and rain rate from Zelinka and Hartmann (2009).

c. Dry versus humid environments

In this section, the *Aqua* composite plots shown above are sorted by environmental humidity derived from the TMI.

The composite CRH shown in Fig. 2 is computed regardless of how moist or dry the surrounding atmosphere is. The effects of environmental humidity, however, may indirectly influence the composite diagram when broken down by the degree of convective organization, since a given class of convective systems could favor one humidity condition more than another. Figure 3 is the histogram of TRMM precipitation coverage separated by different CRHs of the surrounding atmosphere, constructed with simultaneous TRMM measurements of PR-detected convection and TMI-based CWV. It is noted that the histogram is defined and normalized in such a way that it reflects the relative size of the samples that are averaged into each curve presented later in Fig. 4. Scattered cumuli dominate dry environments while organized convective systems tend to be relatively more abundant in moist atmospheres. Dispersion among four curves in Fig. 2 should therefore implicitly reflect the contrast between moist and dry environments to the extent that the moisture environment is correlated with the nature of convective systems allowed to develop in it.

In attempt to separate the effects of moisture and convective organization, the composite diagrams are broken down further by the CRH value at the time of convective development ($t = 0$), or the reference CRH, as an index of the moisture environment (see section 2 for the method to derive the reference CRH). Composite diagrams are constructed separately for well-organized convective systems (TRMM precipitation coverages of 50%–75% and 75%–100% combined together) and less organized systems (TRMM precipitation coverages <50%). Figure 4 shows that the results for organized convective systems (Fig. 4a) and less organized systems (Fig. 4b). One standard deviation around the mean is shaded for the top and bottom curves of composite CRH in Figs. 4a and 4b. While the standard deviation enlarges as t goes away from 0, samples within each reference CRH bin are relatively tightly gathered around the mean in the vicinity of $t = 0$, constituting a distinct population from
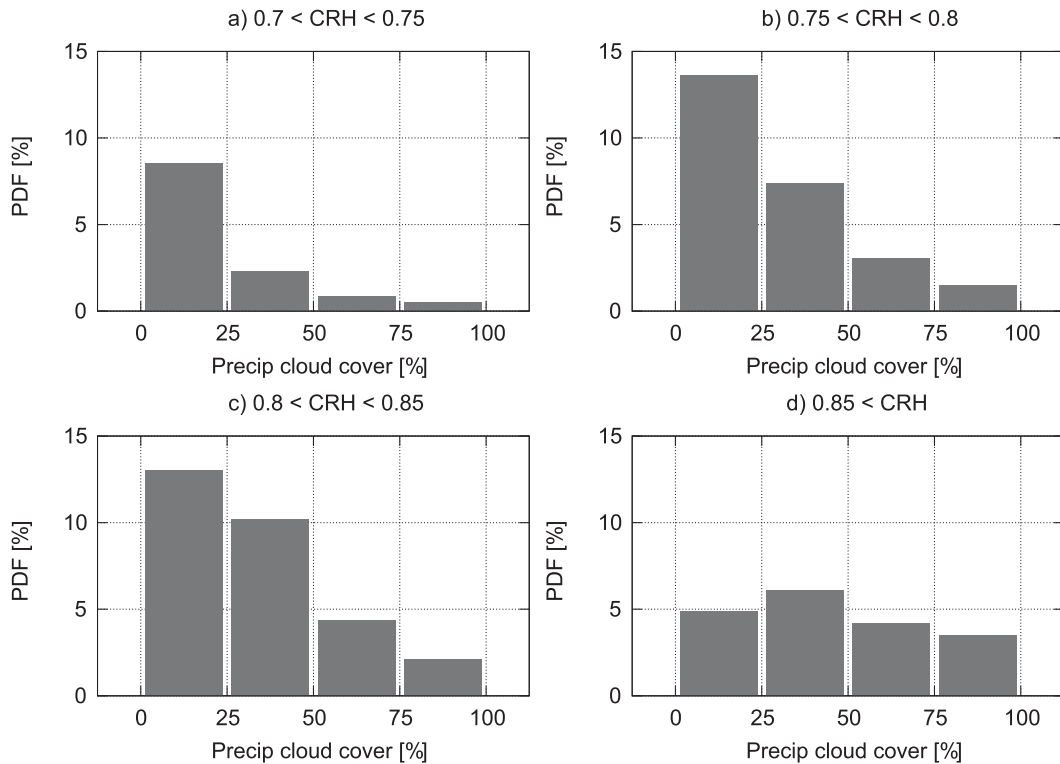
FIG. 3. Histogram of TRMM precipitation coverage for (a) 0.7 < CRH < 0.75, (b) 0.75 < CRH < 0.8, (c) 0.8 < CRH < 0.85, and (d) 0.85 < CRH. The histogram adds up to 100% when all bars in all panels are combined.

each other. This result implies that the reference CRH is a reasonable statistical measure to differentiate a range of humidity environments near the time of convective development.

The qualitative characteristics of the evolution, including the two-stepped drying process after convection, are consistently observed for well-organized convective systems regardless of environmental humidity. Precipitation (Figs. 4c,d) is most enhanced in very humid environments (reference CRHs of 0.85 or higher) and decreases in magnitude as the environment becomes drier. Organized convective systems in the driest environment (the bottom curve in Fig. 4a) exhibit a humidity drop that begins as early as $t \approx -5$ h and ends at $t \approx 0$ when CRH reaches a plateau. This behavior is presumably an artifact, since the base point ($t = 0$) would be forced to find itself somewhat away from the time of maximum humidity when organized systems are conditioned on a very low reference CRH. The peak precipitation rate reaches >2 mm h^{-1} for organized convective systems, while unorganized systems never yield a precipitation rate as high as 1.5 mm h^{-1} even in the most humid environment. This contrast in the peak precipitation results in a characteristic difference between organized and unorganized convective systems when

projected onto the CRH–precipitation plane, as discussed in the next section.

4. Concluding discussion

It was seen in the previous section that precipitation does not start to rise sharply until the steady buildup of moisture reaches within a few hours of its peak as also found by Holloway and Neelin (2010), implying a strong nonlinear correlation between CRH and precipitation. This is confirmed by Fig. 5, where CRH and precipitation paired at each moment from the composite time sequence for various humidity environments (Fig. 4) are mapped into the format devised by Bretherton et al. (2004). Each point, representing a half-hourly mean in the composite domain, proceeds with time as indicated by arrows. Different paths under diverse humidity environments are qualitatively quite similar. The life cycle of organized systems, when projected into the CRH–precipitation plane, first climbs up the path at the far right end until it reaches the top, and then descends along the other path to the bottom where the life cycle is completed (Fig. 5a). The path consists of bifurcated tracks in the nearly vertical sector of the track (hereafter called the high dependence regime), corresponding to
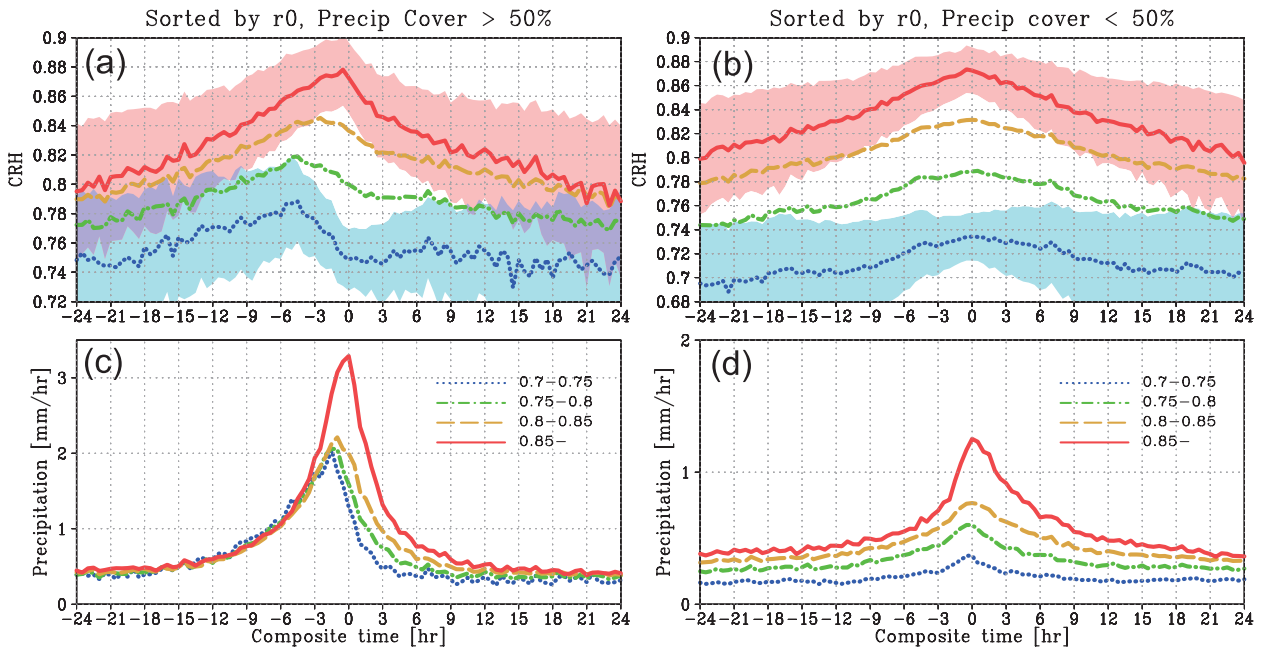
FIG. 4. As in Fig. 2, but stratified by the reference CRH (0.7–0.75, 0.75–0.8, 0.8–0.85, and 0.85–1) for (a),(c) organized (precipitation coverages >50%) and (b),(d) unorganized convective systems (precipitation coverages <50%). One standard deviation around the mean is shaded in (a) and (b): red for the reference CRHs of 0.85–1, blue for 0.7–0.75, and purple where overlapped. No shade is drawn around the other two curves for visual clarity.

the temporal asymmetry about $t = 0$ evident in the composite CRH for well-organized convective systems (Figs. 2a and 4a). Sporadic shallow cumulus, on the other hand, mostly stays on a flat path with little dependence on CRH (hereafter the low dependence regime) as seen in Fig. 5b.

The CRH–precipitation relationship derived from the present composite analysis reflects the short-term variability associated with convective development. For comparison, the climatological relation between CRH and precipitation is plotted together in Fig. 5 (solid line). The short-term variability exhibits a much stronger nonlinearity than the climatology. Precipitation stays lower than the climatology in the low dependence regime of the short-term variability, while precipitation sharply rises far beyond the climatology in the high dependence regime of organized convective systems. The strong nonlinearity as found by Raymond et al. (2007) seems consistent with the short-term variability rather than the climatology. This is reasonable because Raymond et al. (2007) established the CRH–precipitation relation based on instantaneous sounding data and coincident satellite measurements with no temporal averaging.

The climatological relationship may be explained by an ensemble of short-term variations as schematically illustrated in Fig. 6. An organized convective system starts its journey somewhere on the flat path at the bottom and crawls along it as moisture accumulates. The path then turns upward to make a circuit counterclockwise as convection develops and decays before it eventually returns where it started. An unorganized system proceeds initially on the same pathway but reaches only halfway up the ascending path when it turns around to go back the way it came. A sequence of many similar tracks would be aligned across the CRH–precipitation plane as shown in Fig. 6 when a broad range of humidity environments are plotted together. The high and low ends of individual tracks would nearly average each other out when a large number of short-term variations are combined into climatology. The striking dependence on CRH characteristic of the short-term variability would be therefore largely lost in the climatology. Meanwhile, the proportion of organized convective systems relative to less organized ones systematically increases with background humidity (Fig. 3). The climatological mean would be found close to the bottom track in a dry environment where scattered convection dominates precipitation, while heavy precipitation from organized systems would gain an increasing weight in the climatology as the environment moistens. The nonlinearity in the CRH–precipitation relation survives, though severely smoothed, the averaging operation to climatology owing to the fact that the probability of MCS occurrence (Fig. 3) as well as the intensity of individual convective systems (Figs. 5b,c)
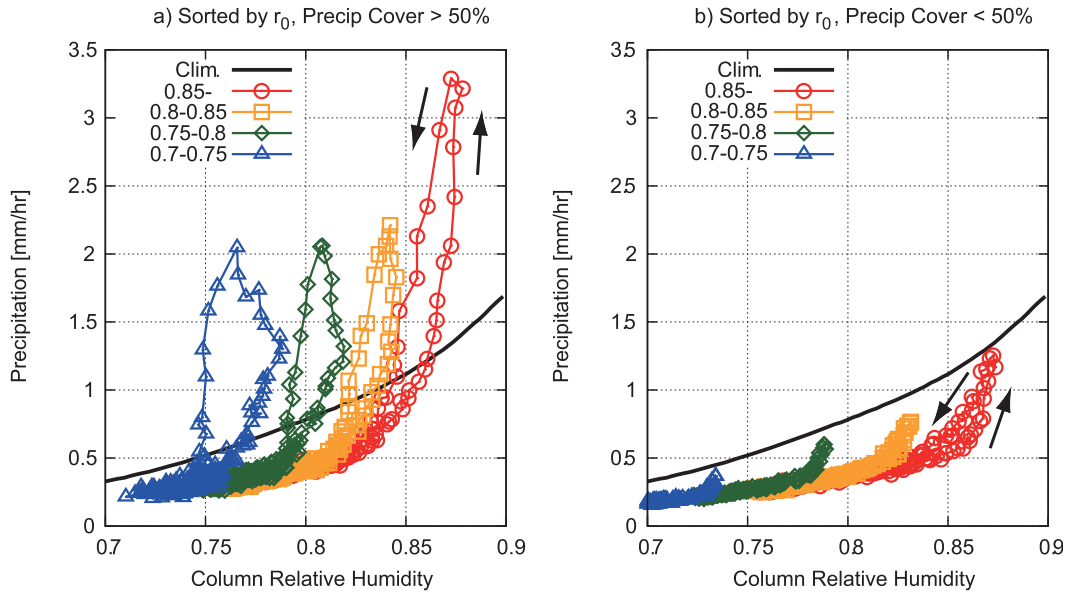
FIG. 5. Relationship between CRH (abscissa) and precipitation rate (ordinate). (a) organized systems (precipitation coverages >50%) stratified by the reference CRH (Figs. 4a,c). (b) As in (a), but for unorganized systems (precipitation coverages <50%; Figs. 4b,d). Different symbols denote separate composite sequences as indicated in each panel, where numbers define the reference CRH. Points on each line are spaced at every 0.5 h for $t = \pm 48$ h. Climatology (i.e., without TRMM-based screening) computed from the present dataset is shown as a solid line.

statistically enhances as the background humidity is increased.

There are some caveats for Fig. 6. It is impractical to repeat the present composite analysis so many times as to compute a whole spectrum of trajectories rather than only eight representatives as plotted in Fig. 5, and hence the schematic (Fig. 6) is difficult to directly confirm with actual data. The complete set of the trajectories, if they were obtained, still might not precisely average into the climatology for the reasons below. First, the composite time series are truncated at ± 48 h in this work, while another choice of the length of period could modify the average. Second, composite data samples within neighboring CRH bins are not totally mutually exclusive as implied by overlapped shades in Fig. 4, which could be a source of bias in the climatological mean.

Peters and Neelin (2006) found that precipitation increases with CWV in the tropics once it exceeds a critical point, while the variability of precipitation peaks near the criticality. Although the critical CWV varies with tropospheric temperature, the mean and variance of precipitation as a function of CWV collapse into a virtually identical curve when normalized by the critical value (Neelin et al. 2009). This universality may correspond to the self-similarity in a family of the CRH–precipitation tracks obtained in the current work (Fig. 5). Precipitation along a trajectory of deep, organized convective systems (Fig. 5a) rapidly rises once CRH exceeds a certain

"criticality," and the paths reaching the precipitation maximum are so steep that precipitation would have a very large variance when averaged for a CRH just above the criticality. The striking precipitation variance noted by Peters and Neelin (2006) might therefore arise in part from the rainfall variability during the course of the convective life cycle. If so, organized convective
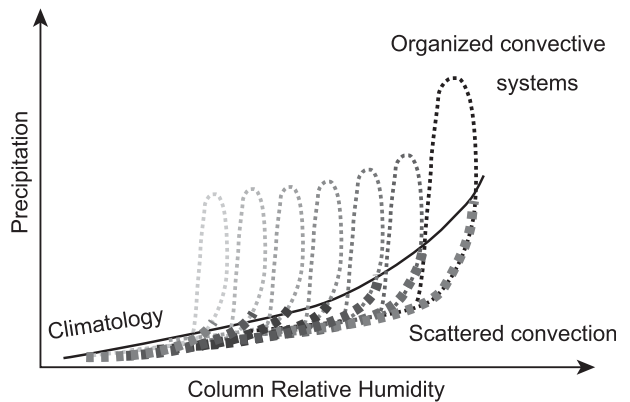

FIG. 6. Schematic relationship between CRH (abscissa) and precipitation (ordinate) for reference to Fig. 5. Dashed tracks delineate short-term variability under different humidity conditions, where thin (thick) lines represent organized (scattered) convection. Grayscale is a rough measure of the frequency of occurrence with higher frequencies shaded more densely (see Fig. 3). Climatology is shown as a solid line.

systems would possibly play a key role in the phase transition to strong convection as hypothesized by Peters and Neelin (2006) and Peters et al. (2009).

Outstanding problems include identifying the mechanisms that give rise to the temporal asymmetry in CRH that is present only for deep, organized convective systems. The present findings, furthermore, give little insight into the origins of an exponential tail extending beyond the criticality in the frequency of CWV occurrence as discussed by Peters and Neelin (2006). These issues are left for future studies to address.

REFERENCES

Bretherton, C. S., M. E. Peters, and L. E. Back, 2004: Relationships between water vapor path and precipitation over the tropical oceans. *J. Climate,* **17,** 1517–1528.

Brown, R. G., and C. D. Zhang, 1997: Variability of midtropospheric moisture and its effect on cloud-top height distribution during TOGA COARE. *J. Atmos. Sci.,* **54,** 2760–2774.

Derbyshire, S. H., I. Beau, P. Bechtold, J. Y. Grandpeix, J. M. Piriou, J. L. Redelsperger, and P. M. M. Soares, 2004: Sensitivity of moist convection to environmental humidity. *Quart. J. Roy. Meteor. Soc.,* **130,** 3055–3079.

Holloway, C. E., and J. D. Neelin, 2009: Moisture vertical structure, column water vapor, and tropical deep convection. *J. Atmos. Sci.,* **66,** 1665–1683.

——, and ——, 2010: Temporal relations of column water vapor and tropical precipitation. *J. Atmos. Sci.,* **67,** 1091–1105.

Kummerow, C. D., W. Barnes, T. Kozu, J. Shiue, and J. Simpson, 1998: The Tropical Rainfall Measuring Mission (TRMM) sensor package. *J. Atmos. Oceanic Technol.,* **15,** 809–817.

——, and Coauthors, 2001: The evolution of the Goddard Profiling Algorithm (GPROF) for rainfall estimation from passive microwave sensors. *J. Appl. Meteor.,* **40,** 1801–1820.

Mapes, B., R. Milliff, and J. Morzel, 2009: Composite life cycle of maritime tropical mesoscale convective systems in scatterometer and microwave satellite observations. *J. Atmos. Sci.,* **66,** 199–208.

Masunaga, H., 2012: A satellite study of the atmospheric forcing and response to moist convection over tropical and subtropical oceans. *J. Atmos. Sci.,* **69,** 150–167.

Neelin, J. D., O. Peters, and K. Hales, 2009: The transition to strong convection. *J. Atmos. Sci.,* **66,** 2367–2384.

Numaguti, A., R. Oki, K. Nakamura, K. Tsuboki, N. Misawa, T. Asai, and Y. M. Kodama, 1995: 4-5-day-period variation and low-level dry air observed in the equatorial western Pacific during the TOGA-COARE IOP. *J. Meteor. Soc. Japan,* **73,** 267–290.

Peters, O., and J. D. Neelin, 2006: Critical phenomena in atmospheric precipitation. *Nat. Phys.,* **2,** 393–396, doi:10.1038/nphys314.

——, ——, and S. W. Nesbitt, 2009: Mesoscale convective systems and critical clusters. *J. Atmos. Sci.,* **66,** 2913–2924.

Raymond, D. J., 2000: Thermodynamic control on tropical rainfall. *Quart. J. Roy. Meteor. Soc.,* **126,** 889–898.

——, S. L. Sessions, and Ž. Fuchs, 2007: A theory for the spinup of tropical depressions. *Quart. J. Roy. Meteor. Soc.,* **133,** 1743–1754.

——, ——, and C. López Carrillo, 2011: Thermodynamics of tropical cyclogenesis in the northwest Pacific. *J. Geophys. Res.,* **116,** D18101, doi:10.1029/2011JD015624.

Sherwood, S. C., 1999: Convective precursors and predictability in the tropical western Pacific. *Mon. Wea. Rev.,* **127,** 2977–2991.

Susskind, J., C. D. Barnet, and J. M. Blaisdell, 2003: Retrieval of atmospheric and surface parameters from AIRS/AMSU/HSB data in the presence of clouds. *IEEE Trans. Geosci. Remote Sens.,* **41,** 390–409.

——, ——, ——, L. Iredell, F. Keita, L. Kouvaris, G. Molnar, and M. Chahine, 2006: Accuracy of geophysical parameters derived from Atmospheric Infrared Sounder/Advanced Microwave Sounding Unit as a function of fractional cloud cover. *J. Geophys. Res.,* **111,** D09S17, doi:10.1029/2005JD006272.

Wentz, F. J., and T. Meissner, 2000: AMSR ocean algorithm: Algorithm theoretical basis document. Remote Sensing Systems, 59 pp.

Zelinka, M. D., and D. L. Hartmann, 2009: Response of humidity and clouds to tropical deep convection. *J. Climate,* **22,** 2389–2404.